



**HAL**  
open science

# Biocatalyst and continuous microfluidic reactor for an intensified production of n-butyl levulinate: kinetic model assessment

Alexandre Cordier, Marcel Klinksiek, Christoph Held, Julien Legros,  
Sébastien Leveneur

## ► To cite this version:

Alexandre Cordier, Marcel Klinksiek, Christoph Held, Julien Legros, Sébastien Leveneur. Biocatalyst and continuous microfluidic reactor for an intensified production of n-butyl levulinate: kinetic model assessment. *Chemical Engineering Journal*, In press, 10.1016/j.cej.2022.138541 . hal-03748632

**HAL Id: hal-03748632**

**<https://normandie-univ.hal.science/hal-03748632v1>**

Submitted on 9 Aug 2022

**HAL** is a multi-disciplinary open access archive for the deposit and dissemination of scientific research documents, whether they are published or not. The documents may come from teaching and research institutions in France or abroad, or from public or private research centers.

L'archive ouverte pluridisciplinaire **HAL**, est destinée au dépôt et à la diffusion de documents scientifiques de niveau recherche, publiés ou non, émanant des établissements d'enseignement et de recherche français ou étrangers, des laboratoires publics ou privés.

1 Biocatalyst and continuous microfluidic reactor for an intensified production of *n*-butyl  
2 levulinate: kinetic model assessment

3 Alexandre Cordier<sup>1</sup>, Marcel Klinksiek<sup>3</sup>, Christoph Held<sup>3</sup>, Julien Legros<sup>1\*</sup>, Sébastien  
4 Leveneur<sup>2\*</sup>

5 <sup>1</sup>*INSA Rouen, CNRS, Normandie Université, UNIROUEN, COBRA laboratory, F-*  
6 *76000 Rouen, France, E-mail: [julien.legros@univ-rouen.fr](mailto:julien.legros@univ-rouen.fr)*

7 <sup>2</sup>*INSA Rouen, UNIROUEN, Normandie Univ, LSPC, UR4704, 76000 Rouen, France,*  
8 *E-mail: [sebastien.leveneur@insa-rouen.fr](mailto:sebastien.leveneur@insa-rouen.fr)*

9 <sup>3</sup> *Laboratory of Thermodynamics, Department of Biochemical and Chemical*  
10 *Engineering, TU Dortmund University, Emil-Figge. Str.70, 44227 Dortmund, Germany*

11

12 **Abstract**

13 The use of enzymes to catalyze chemical reactions has increased these recent years.  
14 Several models have been developed to express the kinetics over these biocatalysts.  
15 The most well-known of them, Michaelis-Menten, is used when only one substrate  
16 adsorbs on the enzyme. In the case of the esterification reaction, i.e., bimolecular  
17 system, a more complex kinetic model such as the Ping-Pong Bi-Bi should be applied.  
18 The use of such advanced models is essential for reactor scaleup and to optimize  
19 production. However, these models usually do not consider the reaction temperature.  
20 To fill this gap, a Ping-Pong Bi-Bi model was developed to produce butyl levulinate  
21 from the esterification of levulinic acid over an immobilized enzyme, Novozym®435.  
22 Microfluidic technology was used to ensure ideal mixing conditions. The Ping-Pong  
23 model, considering inhibition mechanisms, fits the experimental concentrations. ePC-  
24 SAFT equation of state was used to estimate the equilibrium constants.

25 **Keywords**

26 Kinetic modeling, ePC-SAFT, Enzyme, Ping-Pong mechanism

27

## 28        **1. Introduction**

29        Lignocellulosic biomass (LCB) is seen as the best alternative to fossil raw materials to  
30        make the chemical and fuel industries sustainable [1–3]. Compared to first-generation  
31        biomass, LCB is not competing with the food sector, avoiding the fuel versus food  
32        dilemma. The chemistry of this LCB valorization focuses on the production of platform  
33        molecules [4–6] and lignin valorization [4–6].

34        The platform molecule levulinic acid production has gained much interest these last  
35        years [7–9]. Levulinic acid or alkyl levulinates are starting materials for producing  
36        another platform molecule  $\gamma$ -valerolactone (GVL) [10–17]. Alkyl levulinates can be  
37        used directly as blending components for biodiesel or as a fuel oxygenate additives  
38        [18,19], and can also find applications as additives, solvents, and intermediates in fine  
39        chemistry [9]. In the study of Christensen et al., they showed that butyl levulinate (BL)  
40        improved conductivity, cold flow properties, and lubricity of diesel fuel and reduced its  
41        vapor pressure [20]. Moreover, it was found that BL remains in solution with diesel  
42        down to the fuel cloud point and has more compatibility with elastomers, compared to  
43        ethyl levulinate, which tends to separate from diesel at a temperature below 0 °C and  
44        results to be more corrosive [20]. Frigo et al., demonstrated that diesel fuel blended  
45        with a mixture of dibutyl ether and BL could reduce particulate emissions without  
46        changing engine power efficiency or increasing the NO<sub>x</sub> emission [21].

47        Alkyl levulinates can be produced via the alcoholysis of sugar monomers or LA  
48        esterification [7,8,22]. The latter route can be done via homogenous [23],  
49        heterogeneous [24–30] or enzymatic catalysis [31–37]. The use of heterogeneous  
50        catalysts such as resins, zeolite or immobilized enzymes should be favored to avoid  
51        additional separation stages [23]. From a chemical engineering viewpoint, using a  
52        continuous reactor for biomass valorization should be favored for large production [38].

53 Microreactor or microfluidic technology has raised interest in the scientific community  
54 because concentration and temperature gradients are reduced.

55 Production of n-butyl levulinate from LA esterification over lipase catalysis has been  
56 scarcely studied [32,34]. Yadav and Borkar [34] developed a kinetic model of LA  
57 esterification by butanol over Novozym®435, without considering the reversibility of  
58 this reaction or the temperature effect. Bhavsar and Yadav [34] showed that a  
59 continuous packed bed reactor with immobilized Novozym can be used to produce BL.

60 There is a need to intensify this reaction from an industrial [39] and fundamental  
61 standpoint. The use of a microreactor enables to operate in the absence of gradients  
62 allowing to use plug-flow model and thus simplifying the kinetic modeling stage [40].

63 The developed models proposed in the literature for the esterification of carboxylic acid  
64 over enzyme do not consider the temperature effect, and the knowledge of this effect  
65 on kinetic constants is mandatory for an industrial scaleup. In this manuscript, using  
66 microfluidic technology, kinetic models for the synthesis of BL over commercial  
67 Novozym®435 were developed and assessed at different temperatures.

68

69

70

71

72

73

74        **2. Experimental section**

75

76        2.1 Chemicals

77        All the chemicals were used as provided, without further purification. Butan-1-ol (wt%  
78         $\geq 99.9\%$ ), levulinic acid (wt%  $\geq 99\%$ ), (trimethylsilyl)diazomethane (2.0 M in hexane)  
79        and the commercial supported *Candida Antarctica* lipase B (CAL-B), Novozym 435  
80        (5000 U.mg<sup>-1</sup>), were purchased from Sigma-Aldrich. Dichloromethane stabilized by  
81        ethanol was purchased from CARLO ERBA Reagents. Deionized water from the  
82        Aquadem™ system (Veolia) was used.

83        2.2 Analytical method

84        The aliquots taken at each residence time ( $t^R$ ) for the analysis of butyl levulinate  
85        concentration were analyzed on a Thermo Scientific™ TRACE™ 1310 GC-FID  
86        equipped with an apolar column (DB-5MS, 30 m  $\times$  0.250 mm ID  $\times$  0.250  $\mu$ m film  
87        thickness). The initial temperature of the analysis method was set at 50 °C for 2 min to  
88        reach 250 °C with a temperature rate of 25 °C/min. The aliquots were diluted in  
89        dichloromethane, and an excess of trimethylsilyl diazomethane as carboxylic acid  
90        scavenger was added (to protect the GC column from corrosion); 1  $\mu$ L of the resulting  
91        solution was injected into the GC.

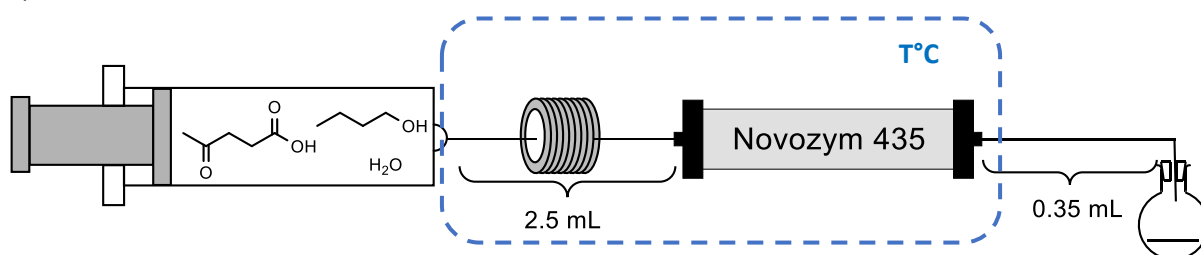
92        High field <sup>1</sup>H NMR analyses were performed on a 300 MHz Bruker Spectrospin  
93        spectrometer. Chemical shifts ( $\delta$ ) are given with regard to TMS using residual CHCl<sub>3</sub>  
94        solvent as an internal reference.

95

96

97 2.3 Procedure for the biocatalyzed esterification of levulinic acid with butanol in a  
98 flow reactor

99 The Luer-lock syringe, filled with levulinic acid, butanol and water, was connected to a  
100 preheating loop (PTFE tubing, ID = 1.59 mm, L = 126 cm) before the packed-bed  
101 reactor with an internal diameter of 6.6 mm. The packed-bed reactor was composed  
102 of an Omnifit™ column filled with Novozym®435 immersed in a thermostated bath (Fig.  
103 1).



104

105 Fig.1. Process for the butyl levulinate synthesis with Omnifit cartridge.  
106

107 The kinetic measurements were performed. First, the flow system was filled with the  
108 solution at a flow rate of 5 mL/min. Then the flow-rate was increased step by step to  
109 reach the desired  $t^R$ . The collection of aliquots began after running the system for 2 mL  
110 of reaction product collected, in order to reach the steady-state. The volume of the  
111 microreactor is related to the amount of the Novozym®435: 50 mg, 100 mg and 150  
112 mg of supported CAL-B were packed 195  $\mu$ L, 390  $\mu$ L and 520  $\mu$ L, respectively. The  
113 kinetic monitoring was performed as described in Table 1.

114

115

Table 1. Different flow-rates used for the kinetic monitoring.

Mass of Novozym®435 (mg) Residence Time (min)	50 mg	100 mg	150 mg
30	6.5 $\mu\text{L}/\text{min}$	13 $\mu\text{L}/\text{min}$	17.33 $\mu\text{L}/\text{min}$
20	9.75 $\mu\text{L}/\text{min}$	19.5 $\mu\text{L}/\text{min}$	26 $\mu\text{L}/\text{min}$
15	13 $\mu\text{L}/\text{min}$	26 $\mu\text{L}/\text{min}$	34.66 $\mu\text{L}/\text{min}$
10	19.5 $\mu\text{L}/\text{min}$	39 $\mu\text{L}/\text{min}$	52 $\mu\text{L}/\text{min}$
7	27.85 $\mu\text{L}/\text{min}$	55.71 $\mu\text{L}/\text{min}$	74.28 $\mu\text{L}/\text{min}$
5	39 $\mu\text{L}/\text{min}$	78 $\mu\text{L}/\text{min}$	104 $\mu\text{L}/\text{min}$
3	65 $\mu\text{L}/\text{min}$	130 $\mu\text{L}/\text{min}$	173.33 $\mu\text{L}/\text{min}$
2	97.5 $\mu\text{L}/\text{min}$	195 $\mu\text{L}/\text{min}$	260 $\mu\text{L}/\text{min}$
1	195 $\mu\text{L}/\text{min}$	390 $\mu\text{L}/\text{min}$	520 $\mu\text{L}/\text{min}$
0	0 $\mu\text{L}/\text{min}$	0 $\mu\text{L}/\text{min}$	0 $\mu\text{L}/\text{min}$

116

117 Repeatability was assessed by collecting three samples after the steady-state, and it  
 118 was found that the standard deviation was lower than  $0.05 \text{ mol}\cdot\text{L}^{-1}$ . Furthermore, one  
 119 run was repeated two times (Run 4) on different days to verify the repeatability of the  
 120 whole system (Fig. S1.1). Fig. S1.1 shows that the repeatability is good.

121 Table 2 shows the experimental matrix used in this study.

122



Table 2. Experimental matrix for esterification.

Run	Temperature (°C)	Mass of catalyst (mg)	Void volume (μL)	Inlet (mol/L)				Ratio [BuOH] <sub>in</sub> /[LA] <sub>in</sub>
				BL	LA	BuOH	W	
1	20	100	390	0.00	2.61	7.81	0.34	3.00
2	35	100	390	0.00	2.61	7.81	0.34	3.00
3	50	100	390	0.00	2.61	7.81	0.34	3.00
4	65	100	390	0.00	2.61	7.82	0.34	3.00
5	80	100	390	0.00	2.61	7.81	0.34	3.00
6	65	150	520	0.00	2.61	7.81	0.34	2.99
7	65	50	195	0.00	2.61	7.81	0.34	2.99
8	65	100	390	0.00	5.09	5.09	0.31	1.00
9	50	100	390	0.00	5.16	5.16	0.32	1.00
10	35	100	390	0.00	5.09	5.09	0.31	1.00
11	20	100	390	0.00	5.09	5.09	0.31	1.00
12	65	150	520	0.00	5.09	5.09	0.31	1.00
13	65	50	195	0.00	5.09	5.09	0.31	1.00
14	65	100	390	0.00	1.74	8.71	0.32	4.99
15	50	100	390	0.00	1.77	8.83	0.33	5.00
16	35	100	390	0.00	1.79	8.95	0.33	4.99
17	20	100	390	0.00	1.82	9.07	0.34	4.99
18	65	50	195	0.00	1.74	8.71	0.32	4.99
19	65	150	520	0.00	1.74	8.71	0.32	4.99
20	65	100	390	0.00	2.59	7.76	0.70	3.00
21	50	100	390	0.00	2.59	7.76	0.70	3.00
22	35	100	390	0.00	2.59	7.76	0.70	3.00
23	20	100	390	0.00	2.59	7.76	0.70	3.00
24	65	100	390	0.00	2.46	7.78	1.20	3.17
25	50	100	390	0.00	2.57	7.69	1.20	3.00
26	35	100	390	0.00	2.46	7.78	1.20	3.17
27	20	100	390	0.00	2.46	7.78	1.20	3.17

## 126 2.4 Stability of Novozym 435

127 It is fundamental to evaluate the Novozym 435 stability to know if there are enzymes  
128 or another product leaching from support denaturation. Two experiments were  
129 performed: a degradability test for Novozym 435 in butanol solvent in a batch reactor  
130 and deactivation in the microfluidic system.

131 The degradability test was performed as follows: 100 mg of Novozym 435 were placed  
132 into 390  $\mu\text{L}$  of a solution containing a  $[\text{BuOH}]_{\text{inlet}}/[\text{LA}]_{\text{inlet}}$  ratio = 5. The mixture was  
133 heated at 65°C. After 1 h, the sample was filtered through a 30  $\mu\text{m}$  PTFE frit of the  
134 Omnifit column (the exact same one that we used for the kinetic study), then  $\text{CDCl}_3$   
135 was added, and a  $^1\text{H}$  NMR analysis was performed. The obtained spectrum was  
136 compared to those of authentic samples of butyl levulinate, n-butanol and levulinic  
137 acid, as well as those from PMMA and methyl methacrylate from the literature [41].

138 The deactivation test was carried out at 65 °C with 100 mg of catalyst and inlet levulinic  
139 acid concentration of 2.61  $\text{mol}\cdot\text{L}^{-1}$ . The outlet concentration of BL was followed with  
140 time-on-stream at 65°C.

### 141 3. Results

#### 142 3.1 External and internal mass transfer evaluation

143 Besides the effect of mass transfer resistance on the kinetics, the presence or absence  
144 of flow maldistribution should be determined [42–44]. According to Doraiswamy and  
145 Tajbl [42], if the ratio reactor diameter on particle diameter is higher than 4, then they  
146 conclude that there is a proper liquid distribution with no channeling. In this system,  
147 this ratio is higher than 10. Thus, we concluded the absence of flow maldistribution.

148 To evaluate the influence of both effect, the same methodology presented by Leveneur  
149 et al. [45] was applied.

150 External mass transfer for each experiment was evaluated throughout the coefficient  
151  $f_e$  (Equation (1)) defined by Villiermaux [46]. If  $f_e$  is lower than 5%, then the external  
152 mass transfer is negligible.

$$153 \quad f_e = \frac{\overline{r_{Obs}} \cdot L}{k_D \cdot C_b} \quad (1)$$

154 where, L is the ratio particle volume ( $V_P$ ) on the external particle surface ( $A_P$ ),  $\overline{r_{Obs}}$  is  
155 the initial observed rate of esterification,  $k_D$  is the mass transfer coefficient and  $C_b$  the  
156 concentration in the bulk phase. In Equation (1), the concentration of LA in the bulk  
157 phase was used because butanol is in excess. The mean particle size of  
158 Novozym®435 is equal to 0.65 mm, and thus L is equal to  $1.08 \cdot 10^{-4}$  m [47].

159 The mass transfer coefficient  $k_D$  can be estimated via the Sherwood number (Sh)  
160 expressed as

$$161 \quad Sh = \frac{k_D \cdot \overline{d_P}}{D} = 2 + 1.8 \cdot Re_P^{\frac{1}{2}} \cdot Sc^{\frac{1}{3}} \quad (2)$$

162 where,  $d_p$  is the mean diameter of the catalyst particle, and Sc stands for the  
163 Schmidt number expressed as

$$164 \quad Sc = \frac{\mu_f}{\rho_f \cdot D} \quad (3)$$

165  $D$  is the molecular diffusion coefficient of LA in butanol calculated by the Wilke-Chang  
166 equation [48]. For instance, the molecular diffusion of LA in butanol at 50°C was found  
167 to be  $9.02 \cdot 10^{-10} \text{ m}^2 \cdot \text{s}^{-1}$ . The terms  $\mu_f$  and  $\rho_f$  represent the viscosity and density of the  
168 fluid, i.e., butanol. These physicochemical properties were calculated from Ariba et al.  
169 work [49]. The  $f_e$  values were found to be lower than 5% for each experiment showing  
170 the absence of external mass transfer.

171 The internal mass transfer effect was evaluated via the Thieles modulus number  $\phi_S$   
172 defined by Equation (4) [46].

$$173 \quad \phi_S^2 = \frac{\overline{r_{Obs}} \cdot L^2}{D_e \cdot C_S} \quad (4)$$

174 If  $\phi'_S$  is lower than 0.1, hence internal mass transfer can be assumed to be negligible.  
175  $C_S$  is the LA concentration at the particle surface and in this study  $C_S=C_B$  because  
176 there is no external mass transfer. The term  $D_e$  represents the effective diffusion  
177 coefficient defined as  $D_e = \frac{\varepsilon_P \sigma}{\tau} \cdot D$ , where  $\varepsilon_P$ ,  $\sigma$  and  $\tau$  represent the porosity,  
178 constriction factor and tortuosity of the particle, respectively. From Ravelo et al. [47],  
179 Novozym<sup>®</sup>435 porosity is equal to 0.5. The tortuosity and constriction factor values  
180 were fixed to 6 and 1 [50]. Based on the  $\phi'_S$  values of each experiment, the internal  
181 mass transfer can be assumed to be negligible.

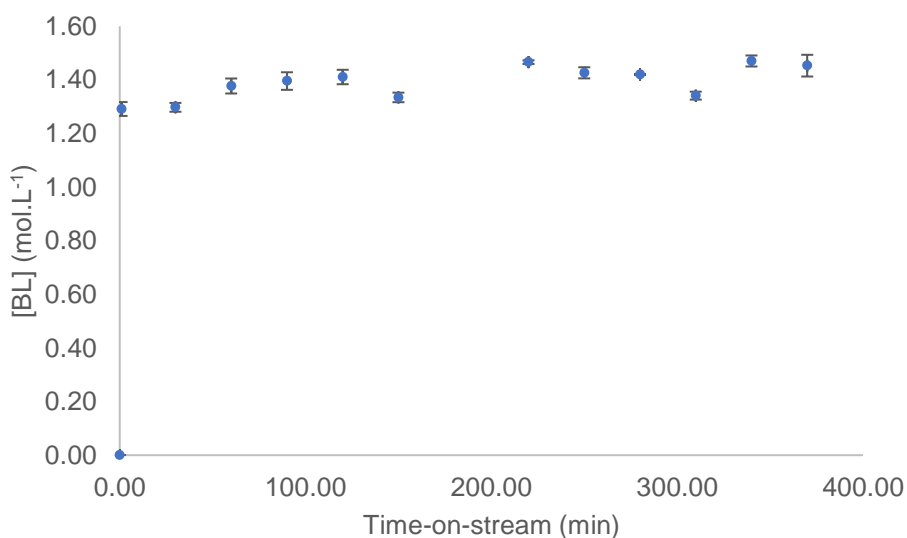
182

183

184 *3.2 Novozym 435 stability study*

185 Novozym 435 degradability test (S2) is an essential study because its acrylic  
186 support/matrix tends to dissolve in many organic solvents [51–53]. By spectrum  
187 comparison of the mixture with a <sup>1</sup>H NMR analysis of different isolated products (butyl  
188 levulinate, n-butanol and levulinic acid), the mixture just contains n-butanol, levulinic  
189 acid and butyl levulinate and absolutely no traces of PMMA (or associate compound)  
190 were detected. Thus, our measurements are perfectly reliable with no interference from  
191 external chemicals.

192 Fig. 2 shows the BL concentration at the outlet versus time-on-stream. From Fig. 2,  
193 one can notice that enzyme deactivation can be neglected during the experiment.



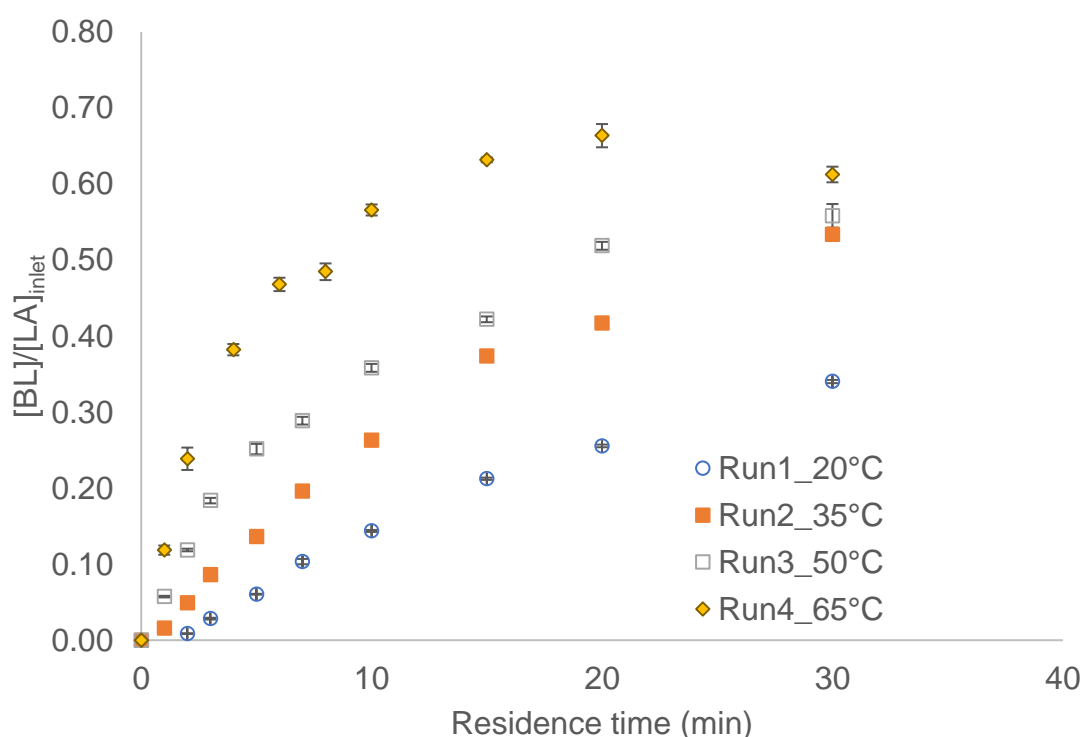
194  
195 Fig. 2. Evolution of experimental BL concentration (blue circle) with error bars (black)  
196 versus time-on-stream at 65°C, [LA]<sub>inlet</sub>=2.61 mol.L<sup>-1</sup> and 100 mg of catalyst.

197 *3.3 Temperature effect*

198 Fig. 3 shows the effect of temperature on the ratio  $\frac{[BL]}{[LA]_{inlet}}$ , where [BL] is the  
199 experimental outlet concentration of BL. To evaluate this effect, experimental data

200 obtained from Runs 1-4 were compared, because there were carried out in the same  
 201 operating conditions, except for the reaction temperature (Table 2). As expected, the  
 202 kinetics of esterification increases with temperature.

203 These data can also be used to evaluate the effect of mass transfer. The natural  
 204 logarithm of the initial rate constants versus  $1/T$  was plotted (Fig. S3.1). From Fig. S3.1,  
 205 the linearity between the natural logarithm of the initial rate constants and  $1/T$  confirms  
 206 the absence of mass transfer resistance.



207  
 208 Fig.3. Effect of temperature on the experimental concentration ratio  $[BL]/[LA]_{inlet}$   
 209 (Table 2): Run 1 at 20 °C (light blue circle), Run 2 at 35 °C (orange square), Run 3 at  
 210 50 °C (grey square), Run 4 at 65 °C (yellow diamond) and error bars (black).

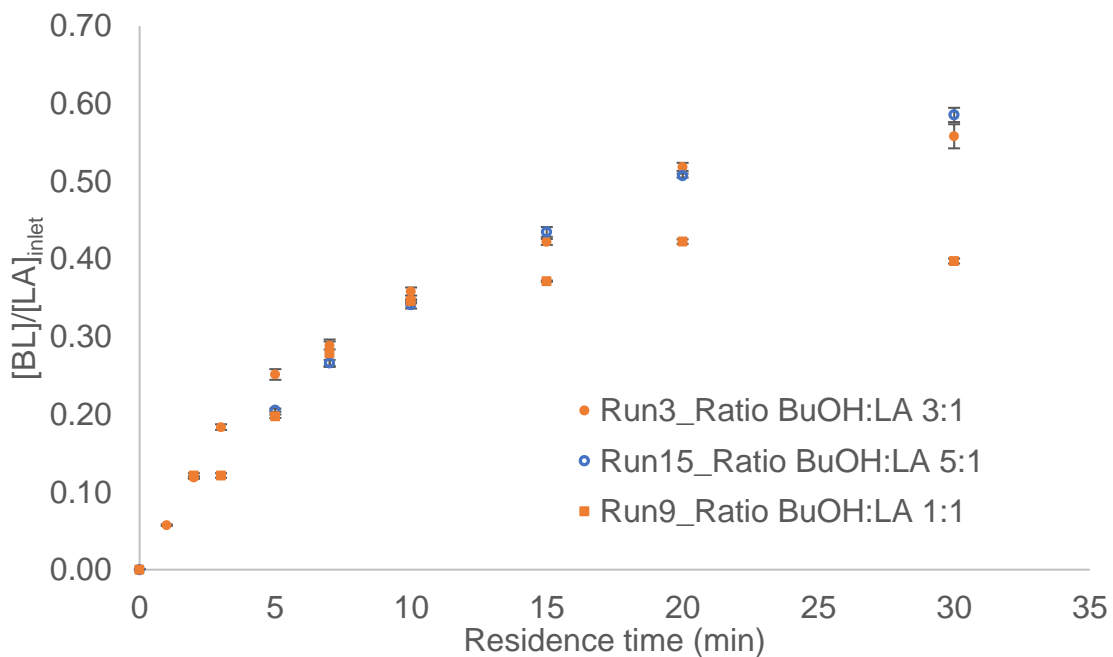
### 211 3.4 Molar ratio effect

212 The effect of  $\frac{[BuOH]_{inlet}}{[LA]_{inlet}}$  can affect the thermodynamics and kinetics of esterification [31].

213 Figs 4 and 5 show the effect of this ratio on the kinetics, via the normalized ratio  $\frac{[BL]}{[LA]_{inlet}}$ .

214 Different experiments carried out in similar operating conditions, except the ratio  
 215  $\frac{[BuOH]_{inlet}}{[LA]_{inlet}}$ , were compared (Table 2). One can notice that when  $\frac{[BuOH]_{inlet}}{[LA]_{inlet}}$  is equal to  
 216 3:1 or 5:1, then the reaction rates and equilibrium values are similar. For a  $\frac{[BuOH]_{inlet}}{[LA]_{inlet}}$   
 217 equal to 1:1, there is a deviation when the reaction reaches the equilibrium.

218



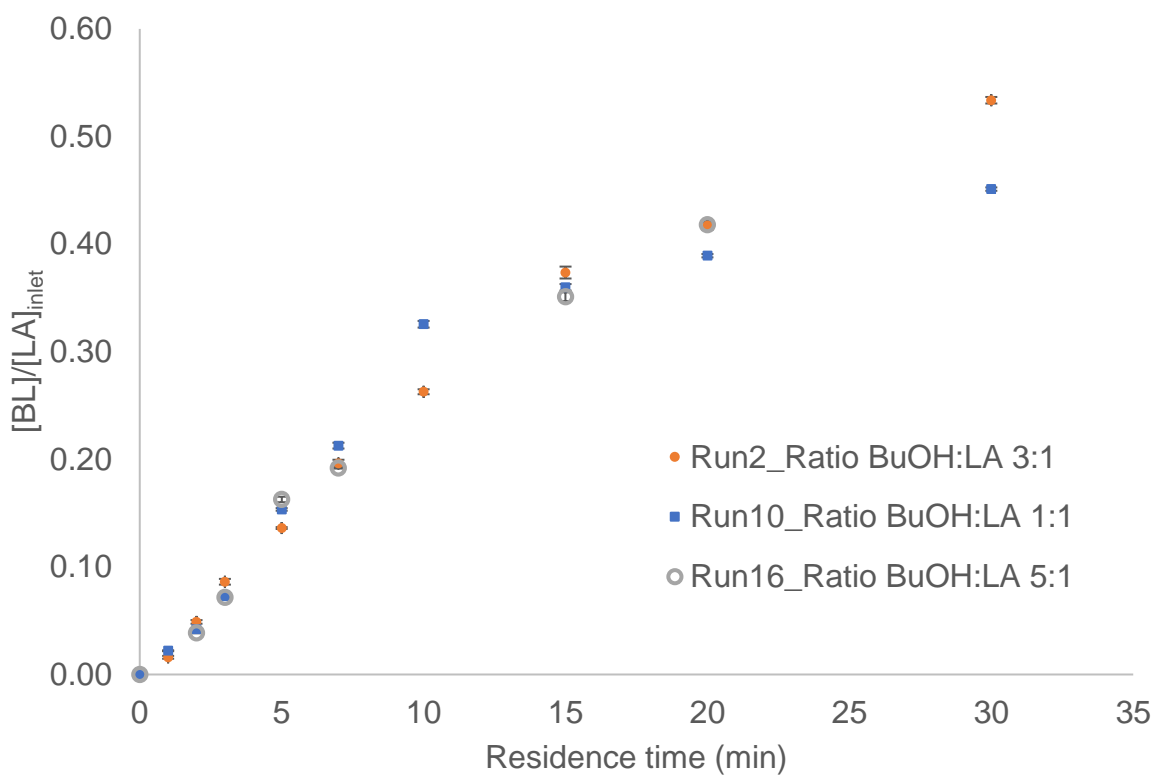
219

220 Fig.4. Effect of  $\frac{[BuOH]_{inlet}}{[LA]_{inlet}}$  ratio on experimental concentration ratio  $[BL]/[LA]_{inlet}$  at 50°C

221 (Table 2): Run 3 at  $\frac{[BuOH]_{inlet}}{[LA]_{inlet}} = 3:1$  (orange circle), Run 15 at  $\frac{[BuOH]_{inlet}}{[LA]_{inlet}} = 5:1$  (blue

222 circle), Run 9 at  $\frac{[BuOH]_{inlet}}{[LA]_{inlet}} = 1:1$  (orange square) and error bars (black).

223



224

225 Fig.5. Effect of  $\frac{[BuOH]_{inlet}}{[LA]_{inlet}}$  ratio on experimental concentration ratio  $[BL]/[LA]_{inlet}$  at 35

226 °C (Table 2): Run 2 at  $\frac{[BuOH]_{inlet}}{[LA]_{inlet}} = 3:1$  (orange circle), Run 10 at  $\frac{[BuOH]_{inlet}}{[LA]_{inlet}} = 1:1$

227 (blue square), Run 16 at  $\frac{[BuOH]_{inlet}}{[LA]_{inlet}} = 1:1$  (grey circle) and error bars (black).

228



### 229 3.5 Evaluation of equilibrium constant

230 The PC-SAFT equation of state first published by Gross and Sadowski [54]  
231 expresses the residual Helmholtz energy  $a^{res}$  as shown in Equation 5.

$$232 \quad a^{res} = a^{hc} + a^{disp} + a^{assoc} \quad (5)$$

233 Thereby the hard-chain ( $a^{hc}$ ) reference system represents the repulsive interactions  
234 between the molecules. The attractive interactions, such as the dispersion ( $a^{disp}$ ),  
235 association ( $a^{assoc}$ ), are described as perturbations of the reference system. More  
236 details on the modeling procedure and parameters used can be found in  
237 Supplementary Information (S4). Thermodynamic modeling of the reaction equilibrium  
238 is based on the temperature and pressure-dependent equilibrium constant  $K_{th}$ . It is  
239 calculated by the reacting agent concentrations in the equilibrium and activity  
240 coefficients according to Equation 6.

241 Based on Equation 5, we can calculate the temperature and pressure-dependent  
242 equilibrium constant  $K_{th}$ .

$$243 \quad K_{th}(T, p) = K_{eq}(T, p, x) \cdot K_{\gamma}(T, p, x) = \prod_i (x_i \cdot \gamma_i)^{\nu_i} \quad (6)$$

244 where,  $K_{eq}$  is determined from the experimental equilibrium concentrations and the  
245 activity coefficients are obtained by PC-SAFT [54–59]. The activity coefficient of each  
246 reactant  $i$  in the mixture is calculated from the ratio of the fugacity coefficients in the  
247 mixture and of the fugacity coefficient of the pure component.

$$248 \quad \gamma_i = \frac{\varphi_i(T, p, x)}{\varphi_{oi}(T, p, x_i=1)} \quad (7)$$

249 The equilibrium constant  $K_{th}$  for each temperature enables the calculation of  
250 equilibrium concentrations at different conditions, i.e., molar ratios. The equilibrium

251 constant  $K_{th}$  was calculated based on the experiments with a molar ratio of BuOH:LA  
252 3:1 (Table 3).

253 Table 3. Calculated equilibrium constant  $K_{th}$  based on the equilibrium concentrations  
254 of Runs 1-5 (Table 2).

T / °C	$K_{eq}$	$K_Y$	$K_{th}$
20	0.157	3.578	0.56
35	0.309	2.793	0.67*
50	0.356	2.308	0.82
65	0.491	1.969	0.97
80	0.695	1.732	1.20

255 \*interpolated value

256

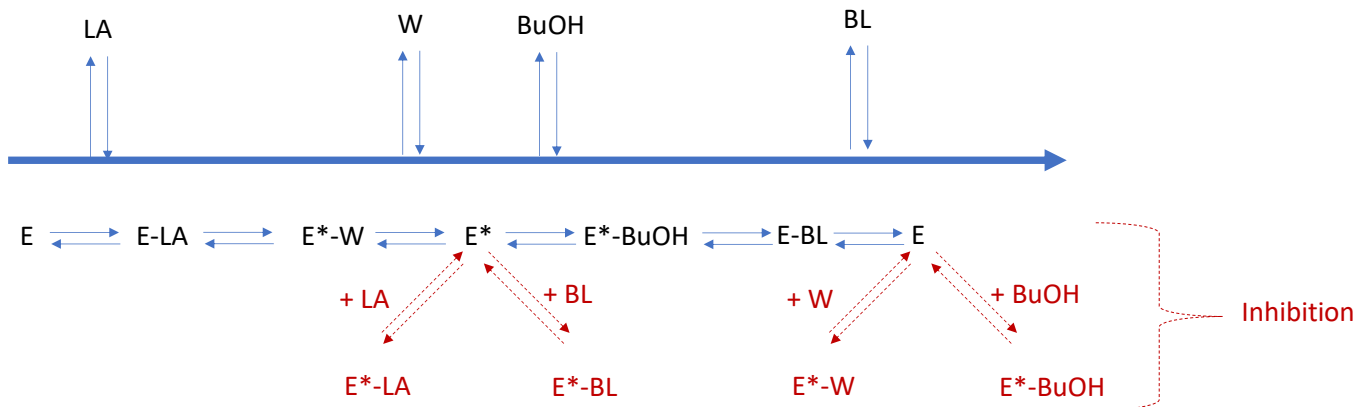
257

258 **4. Discussion**

259 **4.1 Ping-Pong Models**

260 Several authors showed that the Ping-Pong Bi-Bi mechanism can be used for the  
 261 esterification reactions [32,60–66]. Several of them showed that alcohol and carboxylic  
 262 acid can inhibit the enzyme, but none developed a kinetic model considering the  
 263 reversibility of this reaction and the temperature effect on the kinetic constants.

264 Fig. 6 shows the Ping-Pong Bi-Bi mechanism for the esterification of LA by butanol.



265

266 Fig. 6. Ping-Pong Bi-Bi and inhibition mechanism for the esterification of LA.

267 From Varma and Madras study [65], the rate equation can be derived as

268

$$r_{Esterification} = \frac{k_f \cdot k_b \cdot [E]_0^2 \cdot \left( [LA] \cdot [BuOH] - \frac{[BL] \cdot [W]}{K_{eq}} \right)}{D} \quad (8)$$

269 where,  $[LA]$ ,  $[BuOH]$ ,  $[BL]$  and  $[W]$  are the outlet concentrations of levulinic acid,  
 270 butanol, butyl levulinate and water, respectively. The term  $[E]_0$  stands for the initial  
 271 concentration of enzyme. The denominator D is expressed as

$$\begin{aligned}
D = & k_b \cdot [E]_0 \cdot [LA] \cdot [BuOH] + k_b \cdot [E]_0 \cdot K_{BuOH} \cdot [LA] \cdot \left(1 + \frac{[LA]}{K_{ILA}}\right) \\
& + k_b \cdot [E]_0 \cdot K_{LA} \cdot [BuOH] \cdot \left(1 + \frac{[BuOH]}{K_{IBuOH}}\right) + \frac{k_f \cdot [E]_0 \cdot K_W}{K_{eq}} \cdot [BL] \cdot \left(1 + \frac{[BL]}{K_{IBL}}\right) \\
& + \frac{k_f \cdot [E]_0 \cdot K_{BL}}{K_{eq}} \cdot [W] \cdot \left(1 + \frac{[W]}{K_{IW}}\right) \\
& + \frac{k_f \cdot [E]_0}{K_{eq}} \cdot [W] \cdot [BL] + \frac{k_f \cdot K_{BL} \cdot [E]_0}{K_{IIA} \cdot K_{eq}} \cdot [W] \cdot [LA] + \frac{k_b \cdot K_{LA} \cdot [E]_0}{K_{IIBL}} \cdot [LA] \cdot [BL] \\
& + \frac{k_b \cdot K_{LA} \cdot [E]_0}{K_{BuOH-W}} \cdot [W] \cdot [BuOH] + \frac{k_b \cdot K_{BuOH} \cdot [E]_0}{K_{LA-BL}} \cdot [LA] \cdot [BL] \quad (9)
\end{aligned}$$

273 The terms  $k_f \cdot [E]_0$  and  $k_b \cdot [E]_0$  represent kinetic rate constants. The terms  $K_{LA}$ ,  $K_{BL}$ ,  
274  $K_{BuOH}$  and  $K_W$  are the Michaelis constants for LA, BL, BuOH, and W, respectively. The  
275 inhibition constants by levulinic acid and BL are defined by  $K_{IIA}$  and  $K_{IIBL}$ . The  
276 dissociation constants, representing the dissociation of the inhibitor from the  
277 corresponding enzyme-inhibitor, are  $K_{ILA}$ ,  $K_{IBL}$ ,  $K_{IBuOH}$  and  $K_{IW}$ . The adsorption  
278 constants  $K_{BuOH-W}$  and  $K_{LA-BL}$  are lumped constants.

279 Mitchell and Krieger proposed a new rate expression of this Ping-Pong Bi-Bi  
280 mechanism [63],

$$r_{Esterification} = \frac{(k_{LA} \cdot [LA] \cdot k_{BuOH} \cdot [BuOH] - k_{BL} \cdot [BL] \cdot k_W \cdot [W]) \cdot [E]_0}{D'} \quad (10)$$

282 where, the denominator  $D'$  is

$$\begin{aligned}
D' = & k_{LA} \cdot [LA] \cdot \left(1 + \frac{[W]}{K_{IW}} + \frac{[BuOH]}{K_{BuOH}}\right) + k_{BuOH} \cdot [BuOH] + k_W \cdot [W] \\
& + k_{BL} \cdot [BL] \cdot \left(1 + \frac{[W]}{K_W} + \frac{[BuOH]}{K_{IBuOH}}\right) \quad (11)
\end{aligned}$$

284

285

286 The terms  $k_{LA}$ ,  $k_{BuOH}$ ,  $k_{BL}$  and  $k_W$  are the specific constants of the enzyme for levulinic  
 287 acid, butanol, butyl levulinate and water, respectively.  $K_{BuOH}$  and  $K_W$  are Michaelis-  
 288 type constants for butanol and water, respectively.  $K_{IBuOH}$  and  $K_{IW}$  are the inhibition  
 289 constants for butanol and water, respectively.

290 By considering the binding of BuOH or water with the free enzyme, D' becomes D''

$$291 \quad D'' = k_{LA} \cdot [LA] \cdot \left(1 + \frac{[W]}{K_{IW}} + \frac{[BuOH]}{K_{BuOH}}\right) + (k_{BuOH} \cdot [BuOH] + k_W \cdot [W]) \cdot \left(1 + \frac{[BuOH]}{K_{siBuOH}}\right) \cdot \left(1 + \frac{[W]}{K_{siW}}\right) \\ + k_{BL} \cdot [BL] \cdot \left(1 + \frac{[W]}{K_W} + \frac{[BuOH]}{K_{IBuOH}}\right) \quad (12)$$

292 where,  $K_{siBuOH}$  and  $K_{siW}$  stand for the constants between BuOH and water with the  
 293 free enzyme.

294 According to Mitchell and Krieger [63], these equations are mathematically symmetric  
 295 and less-lumped parameters. Different models were evaluated based on reaction rates  
 296 developed by Mitchell and Krieger [63] and Varma and Madras [65].

#### 297 4.2 Kinetic modeling

298 Experiments were performed in isothermal conditions, and internal and external mass  
 299 transfers were found to be negligible. Plug-flow model was used; thus, material  
 300 balances for each species can be written as

$$301 \quad \frac{d[BL]}{d\tau} = r_{Esterification} \quad (13)$$

$$302 \quad \frac{d[BuOH]}{d\tau} = -r_{Esterification} \quad (14)$$

$$303 \quad \frac{d[LA]}{d\tau} = -r_{Esterification} \quad (15)$$

$$304 \quad \frac{d[W]}{d\tau} = r_{Esterification} \quad (16)$$

305 where,  $\tau$  is the space time defined as  $\frac{V_L}{Q}$ ,  $V_L$  and  $Q$  are the volume of the liquid in the  
306 reactor and volumetric flow-rate, respectively.

307 Ordinary differential equations ODEs (13)-(16) were solved by the solver DDALPUS  
308 algorithm, via a damped Newton method [67].

309 For the non-linear regression, the concentration of BL was used as an observable. The  
310 estimation of the different kinetic constants (Equations (8)-(12)) was done via the  
311 minimization of the objective function  $S(\theta)$  expressed as

$$312 \quad S(\theta) = \sum_{u=1}^n w_u \cdot ([BL]_{exp,u} - [BL]_{sim,u})^2 = SSR \quad (17)$$

313 where,  $w_u$  is the weigh factor for the experimental value  $u$ .

314 The objective function is expanded as a quadratic function of the parameters around  
315 the initial parameter values of the current iteration. The resulting quadratic minimization  
316 problem is solved with a modified Gauss-Jordan algorithm within a user-defined  
317 feasible region; then, a weak line search is conducted to establish an improved  
318 objective value and initial parameter vector for the next iteration. Interval estimates for  
319 the individual estimated parameters are then calculated from the final quadratic  
320 expansion of the objective function. This minimization is done by the package  
321 GREGPLUS to provide optimal parameter estimates with the 95% confidence  
322 intervals, expressed by the highest probability density (HPD). GREGPLUS provides  
323 the normalized parameter covariance matrix.

324 The GREGPLUS package and DDAPLUS solver are implemented in the Athena Visual  
325 Studio® 14.2 [68] used in this study.

326 Different models were evaluated based on the Ping-Pong Bi-Bi mechanism developed  
 327 by the Varma and Madras study [65] and the Mitchell and Krieger study [63]. The term  
 328  $[E]_0$  was expressed by the catalyst loading  $\rho_{Enzyme}$ , i.e., the mass of catalyst divided by  
 329 the volume of liquid in the reactor.

330 The general equation for esterification can be derived as

$$331 \quad r_{Esterification} = k_{Esterification} \cdot \rho_{Enzyme} \cdot \frac{1}{D} \cdot \left( [LA] \cdot [BuOH] - \frac{[BL] \cdot [W]}{K_{eq}} \right) \quad (18)$$

332 Different models were assessed, as summarized in Table 4.

333 Model 1 is the simplest one, by letting the denominator D equal to 1.

334 Models 2-4 are derived from Varma and Madras. Equation (8) was divided by  $k_b$ . To  
 335 ease the parameter estimation and avoid division by very low number (close to zero)  
 336 or high number, the following modification were included

$$337 \quad K''_{ILA} = \frac{K_{BuOH}}{K_{ILA}}, K''_{IBuOH} = \frac{K_{LA}}{K_{IBuOH}}, K''_W = \frac{K_W}{K_{eq}}, K''_{BL} = \frac{K_{BL}}{K_{eq}}, K''_{IBL} = \frac{K''_W}{K_{IBL}}, K'_W = k_f \cdot K_W \cdot \frac{1}{k_b} \cdot \frac{1}{K_{eq}},$$

$$K''_{IW} = \frac{K''_{BL}}{K_{IW}},$$

$$K'_{BL} = k_f \cdot K_{BL} \cdot \frac{1}{k_b} \cdot \frac{1}{K_{eq}}$$

$$K_{Lump} = \frac{k_f}{k_b \cdot K_{eq}}, K''_{IIBL} = \frac{K_{LA}}{K_{IIBL}}, K''_{BuOH-W} = \frac{K_{LA}}{K_{BuOH-W}} \text{ and } K''_{LA-BL} = \frac{K_{BuOH}}{K_{LA-BL}}$$

338 Model 2 ignores the inhibition mechanism, hence  $K''_{ILA}$ ,  $K''_{IBL}$ ,  $K''_{IW}$ ,  $K''_{IBuOH}$ ,  $K''_{IILA}$ ,  $K''_{IIBL}$ ,  
 339  $K''_{LA-BL}$ , and  $K''_{BuOH-W}$  were fixed to zero.

340 Model 3 considers the inhibition by butanol and ignores the other inhibition mechanism,  
 341 hence  $K''_{ILA}$ ,  $K''_{IBL}$ ,  $K''_{IW}$ ,  $K''_{IILA}$ ,  $K''_{IIBL}$ ,  $K''_{LA-BL}$ , and  $K''_{BuOH-W}$  were fixed to zero.

342 Model 4 considers all inhibition mechanisms.

343 Models 5-6 are derived from Mitchell and Krieger.

344 Model 5 is based on Equation (10) and Equation (11) divided by  $k_{BuOH}$ . The following  
 345 notations are used

$$346 \quad K_{eq} = \frac{k_{LA} \cdot k_{BuOH}}{k_{BL} \cdot k_W}, K_1 = \frac{k_{LA}}{k_{BuOH}}, K_2 = \frac{k_W}{k_{BuOH}}, K_3 = \frac{k_{BL}}{k_{BuOH}}, K''_{IBuOH} = \frac{1}{K_{IBuOH}}, K''_W = \frac{1}{K_W},$$

$$K''_{BuOH} = \frac{1}{K_{BuOH}}, K''_{IW} = \frac{1}{K_{IW}}, K''_{BuOH-W} = \frac{1}{K_{BuOH-W}} \text{ and } K''_{LA-BL} = \frac{1}{K_{LA-BL}}$$

347 Model 6 is based on Equation (10) and divided Equation (12) by  $k_{BuOH}$ . The following  
 348 notations are included

$$349 \quad K''_{siBuOH} = \frac{1}{K_{siBuOH}} \text{ and } K''_{siW} = \frac{1}{K_{siW}} \quad (19)$$

350 Table 4. Kinetic models tested in this study.

Model	Kinetic term	Denominator
Model 1	$k_{Esterification} \cdot \rho_{Enzyme}$	1
Model 2	$k_f \cdot \rho_{Enzyme}$	$[LA] \cdot [BuOH] + K_{BuOH} \cdot [LA]$ $+ K_{LA} \cdot [BuOH]$ $+ K''_W \cdot [BL]$ $+ K''_{BL} \cdot [W]$ $+ K_{Lump} \cdot [W] \cdot [BL]$
Model 3	$k_f \cdot \rho_{Enzyme}$	$[LA] \cdot [BuOH] + K_{BuOH} \cdot [LA]$ $+ K_{LA} \cdot [BuOH] + K''_{IBuOH} \cdot [BuOH]^2$ $+ K''_W \cdot [BL]$ $+ K''_{BL} \cdot [W]$ $+ K_{Lump} \cdot [W] \cdot [BL]$



Model 4	$k_f \rho_{\text{Enzyme}}$	$ \begin{aligned} & [LA] \cdot [BuOH] + K_{BuOH} \cdot [LA] + K''_{ILA} \cdot [LA]^2 \\ & + K_{LA} \cdot [BuOH] + K''_{IBuOH} \cdot [BuOH]^2 \\ & + K''_W \cdot [BL] + K'_{IBL} \cdot [BL]^2 \\ & + K''_{BL} \cdot [W] + K''_{IW} \cdot [W]^2 \\ & + K_{Lump} \cdot [W] \cdot [BL] + K'''_{ILLA} \cdot [W] \cdot [LA] \\ & + K'''_{IIBL} \cdot [LA] \cdot [BL] \\ & + K''_{BuOH-W} \cdot [W] \cdot [BuOH] \\ & + K''_{LA-BL} \cdot [LA] \cdot [BL] \end{aligned} $
Model 5	$k_{LA} \rho_{\text{Enzyme}}$	$ \begin{aligned} & K_1 \cdot [LA] + K''_{IW} \cdot [W] \cdot [LA] + K''_{BuOH} \cdot [BuOH] \cdot [LA] \\ & + [BuOH] + K_2 \cdot [W] \\ & + K_3 \cdot [BL] + K'_W \cdot [W] \cdot [BL] + K'_{IBuOH} \cdot [BuOH] \cdot [BL] \end{aligned} $
Model 6	$k_{LA} \rho_{\text{Enzyme}}$	$ \begin{aligned} & K_1 \cdot [LA] + K''_{IW} \cdot [W] \cdot [LA] + K''_{BuOH} \cdot [BuOH] \cdot [LA] \\ & + ([BuOH] + K_2 \cdot [W]) \cdot (1 + K''_{siBuOH} \cdot [BuOH]) \\ & \cdot (1 + K''_{siW} \cdot [W]) \\ & + K_3 \cdot [BL] + K'_W \cdot [W] \cdot [BL] + K'_{IBuOH} \cdot [BuOH] \cdot [BL] \end{aligned} $

351

352 To decrease the correlation between the pre-exponential factor and activation energy  
353 and ease the parameter estimation stage, the following modified Arrhenius equation  
354 was used [69].

$$355 \quad k_c(T) = \exp \left[ \ln(k_c(T_{ref})) + \frac{E_a}{R \cdot T_{ref}} \cdot \left( 1 - \frac{T_{ref}}{T} \right) \right] \quad (20)$$

356 where,  $T_{ref}$  is a reference temperature which is the average temperature of the  
357 experimental matrix (Table 1).

358 The following constants were estimated:  $\ln(k_c(T_{ref}))$ ,  $\frac{E_a}{R \cdot T_{ref}}$ , Michaelis-Menten and  
359 inhibition constants. Michaelis-Menten and inhibition constants were assumed to be  
360 temperature independent.

361 The effect of the number of estimated parameters on the models was evaluated via  
362 the AIC number standing for Akaike Information Criterion [16,17,70].

$$363 \quad AIC = \text{Number of independant event} \cdot \ln\left(\frac{SSR}{\text{number of independant event}}\right) \\ + 2 \cdot \text{Number of estimated parameters} \quad (21)$$

364

365 *4.3 Modeling results*

366 In the first step, preliminary modeling results showed that some parameters tend to  
367 zero. Thus, these parameters were discarded:

368 -For Model 2,  $K''_W$ ,  $K_{Lump}$  and  $K''_{BL}$  were discarded in the modeling.

369 -For Model 3,  $K_{LA}$ ,  $K''_W$  and  $K''_{BL}$  were not considered.

370 -For Model 4,  $K_{BuOH}$ ,  $K_{LA}$ ,  $K''_W$ ,  $K''_{BL}$ ,  $K_{Lump}$ ,  $K'''_{ILA}$ ,  $K'_{IBL}$ ,  $K''_{IW}$  and  $K'''_{IBL}$  and  $K''_{LA-BL}$  were  
371 neglected.

372 -For Model 5,  $K''_W$ ,  $K''_{IW}$ ,  $K_1$ ,  $K_2$ ,  $K'_{IBuOH}$  and  $K_3$  were neglected.

373 -For Model 6,  $K'_{IBuOH}$ ,  $K''_{IW}$ ,  $K''_{BuOH}$ ,  $K_2$ ,  $K'_W$  and  $K_3$  were neglected.

374 By discarding these parameters, the reduced models are displayed in Table 5. Table  
375 6 is a summary of the modeling output for the different models. SSR is the sum of  
376 squared residuals, the difference between the experimental and simulated  
377 concentrations. AIC values showed that Model 4 is the most probable one (Table 4).  
378 Due to space limitation of the journal, the modeling results of the other models are  
379 displayed in Supporting Information (S5).

380

381

Table 5. Reduced kinetic models for the esterification of levulinic acid over

382

immobilized enzyme.

Model	Kinetic term	Denominator
Model 1	$k_{\text{Esterification}} \cdot \rho_{\text{Enzyme}}$	1
Model 2	$k_f \cdot \rho_{\text{Enzyme}}$	$[LA] \cdot [BuOH] + K_{BuOH} \cdot [LA]$ $+ K_{LA} \cdot [BuOH]$
Model 3	$k_f \cdot \rho_{\text{Enzyme}}$	$[LA] \cdot [BuOH] + K_{BuOH} \cdot [LA]$ $+ K''_{IBuOH} \cdot [BuOH]^2 + K_{Lump} \cdot [W] \cdot [BL]$
Model 4	$k_f \cdot \rho_{\text{Enzyme}}$	$[LA] \cdot [BuOH] + K''_{LA} \cdot [LA]^2$ $+ K''_{IBuOH} \cdot [BuOH]^2$ $+ K''_{BuOH-W} \cdot [W] \cdot [BuOH]$
Model 5	$k_{LA} \cdot \rho_{\text{Enzyme}}$	$K''_{BuOH} \cdot [BuOH] \cdot [LA]$ $+ [BuOH]$
Model 6	$k_{LA} \cdot \rho_{\text{Enzyme}}$	$K_1 \cdot [LA] + ([BuOH]) \cdot (1 + K''_{siBuOH} \cdot [BuOH])$ $\cdot (1 + K''_{siW} \cdot [W])$

383

384

Table 6. Modeling results for each Model.

	Model 1	Model 2	Model 3	Model 4	Model 5	Model 6
SSR	15.85	15.16	14.83	13.66	15.48	14.03
Number of estimated parameters	2	4	5	5	3	5
AIC	-2311.47	-2335.50	-2347.36	-2398.81	-2324.11	-2381.86

385

386

387

388 Table 7 shows the estimated values with their confidence intervals. One can notice  
389 that the confidence intervals for  $\ln(k_c(T_{ref}))$ ,  $\frac{E_a}{R \cdot T_{ref}}$  and  
390  $K''_{ILA}$  are small, meaning that the initial operating condition variation was well designed  
391 to estimate these parameters. Based on our experimental data, it was not possible to  
392 calculate the credible interval for  $K''_{IBuOH}$ , the optimum value was 51.52 mol.L<sup>-1</sup>.

393 Table 7 presents the Normalized parameter covariance matrix for Model 4. According  
394 to Toch et al. [71], two parameters are correlated if their binary correlation coefficient  
395 is higher than 0.95. From Table 8, one can notice that the estimated parameters are  
396 not correlated.

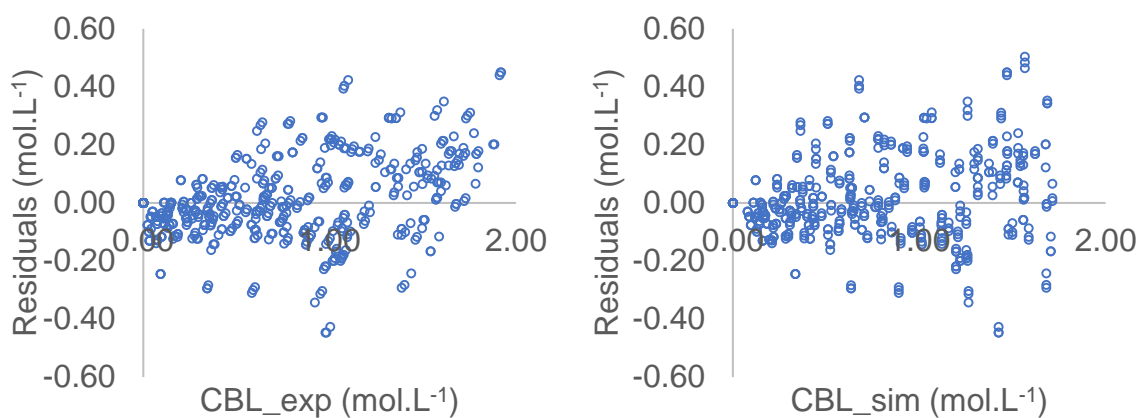
397 Fig. 7 shows that the residuals,  $[BL]_{exp,u} - [BL]_{sim,u}$ , are randomly distributed versus  
398 the experimental concentration of BL ( $[BL]_{exp,u}$ ) and the simulated by Model 4  
399 ( $[BL]_{sim,u}$ ). This means that there are no trends pertaining to the errors.

400 Fig. 8 shows the parity plot, and one can notice that Model 4 can predict the  
401 experimental data correctly.

402 Figs 9 show the fit of model 4 to some experimental concentrations of BL with the 95%  
403 prediction intervals and the mean estimated values. From Figs 9, one can notice that  
404 Model 4 fits well the experimental concentrations, and most of the experimental  
405 concentrations lie between the intervals. The fact that some experimental  
406 concentration points, in the majority at the beginning, are outside the prediction  
407 intervals can be because the LA dissociation is not considered in the modeling or the  
408 adsorption and inhibition terms were not correctly defined.

409 However, the fit of Model 4 to experimental concentration for experiments carried out  
410 with a molar ratio LA/BuOH: 1:1 is lower near to the equilibrium than for the other ratio.

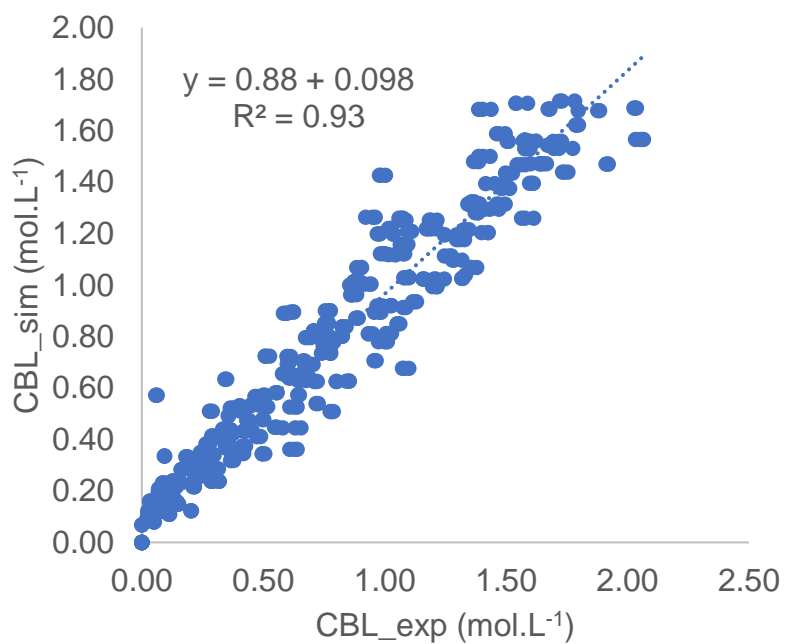
411 This observation is because the equilibrium constant predicted by ePC-SAFT is less  
412 reliable for this ratio.



413

414

Fig. 7. Residual plots for Model 4.



415

416

Fig. 8. Parity plot for Model 4.

417

418

419

420

421 Table 7. Estimated values at  $T_{ref} = 51^\circ\text{C}$  and statistical data for Model 4.

	Units	Estimates	HPD%
$\ln(k_f(T_{ref}))$	$\text{mol}\cdot\text{g}^{-1}\cdot\text{min}^{-1}$	-2.02	6.25
$\frac{Ea_f}{R \cdot T_{ref}}$	-	11.01	5.56
$K''_{ILA}$	$\text{mol}\cdot\text{L}^{-1}$	109.80	19.60
$K''_{BuOH}$	$\text{mol}\cdot\text{L}^{-1}$	51.52	
$K''_{BuOH-W}$	$\text{L}\cdot\text{mol}^{-1}$	148.65	45.13

422

423 Table 8. Normalized parameter covariance matrix for Model 4.

	$\ln(k_f(T_{ref}))$	$\frac{Ea_f}{R \cdot T_{ref}}$	$K''_{ILA}$	$K''_{BuOH-W}$
$\ln(k_f(T_{ref}))$	1			
$\frac{Ea_f}{R \cdot T_{ref}}$	0.1	1		
$K''_{ILA}$	0.69	0.09	1	
$K''_{BuOH-W}$	0.93	0.12	0.53	1

424

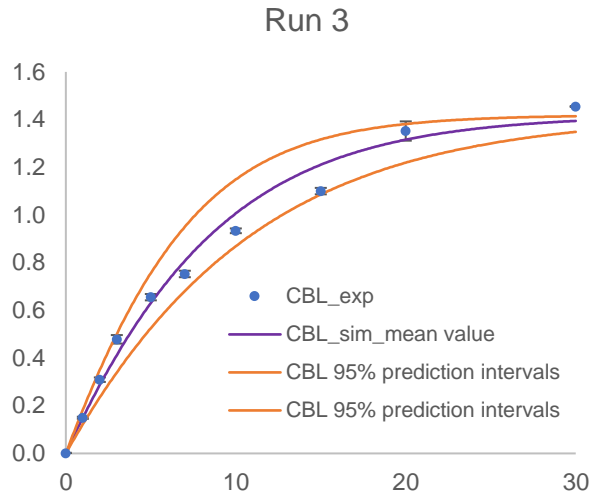
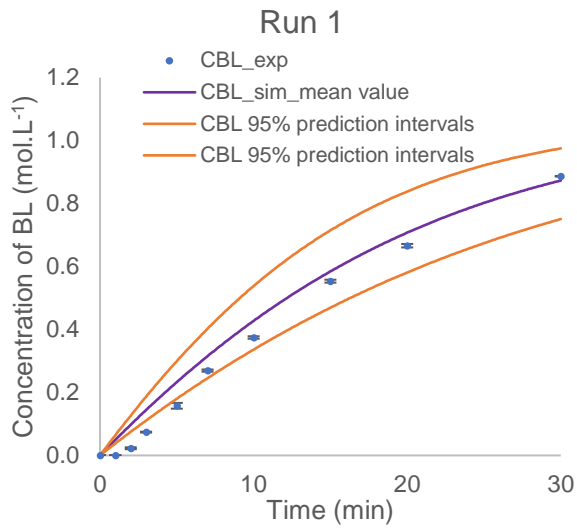
425

426

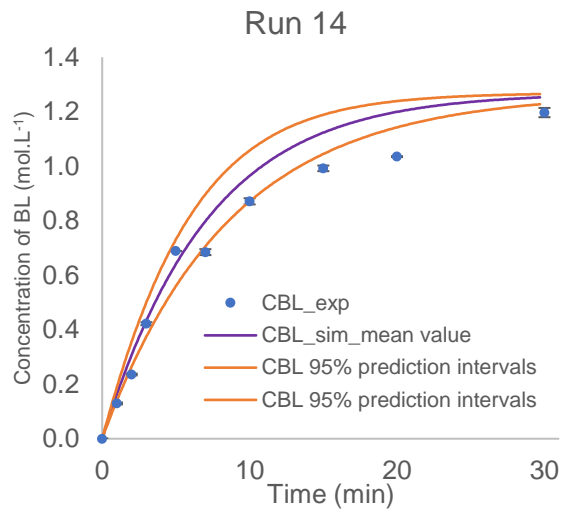
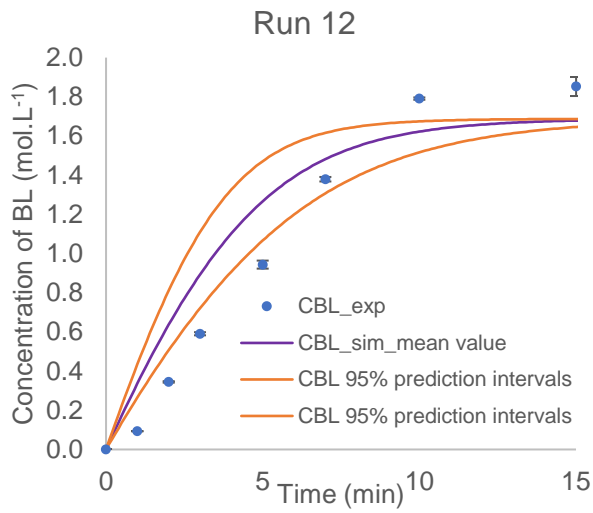
427

428

429



430

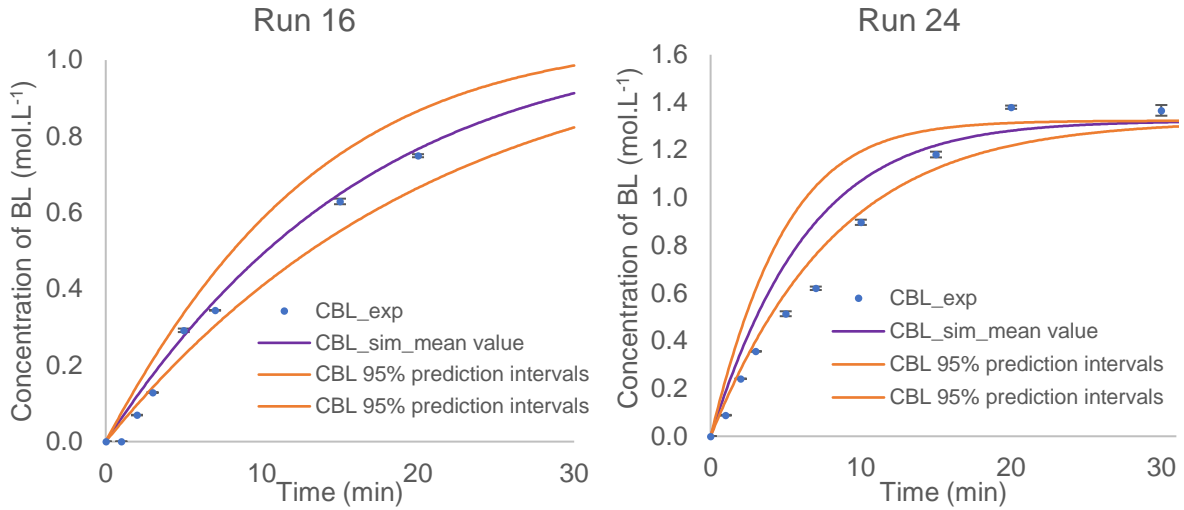


431

432

433





434

435

436

437

438

439

440

Fig. 9. Fit of Model 4 to the experimental concentrations with 95% prediction intervals: experimental concentration of BL (blue circle), error bars (black), simulated concentration of BL using the mean estimated value from Table 7 (purple line), simulated concentration of BL using the estimated values at the extreme of the confidence intervals from Table 7 (orange lines).

441        **5. Conclusions**

442        The synthesis of butyl levulinate from the esterification of levulinic acid over  
443        Novozym®435, an immobilized enzyme, was investigated in microfluidic technology in  
444        isothermal conditions. The enzyme's catalytic activity was found to be stable for 400  
445        minutes. The internal and external mass transfer resistance was found to be negligible.  
446        Thus, a plug-flow model was used to estimate the kinetic constants.

447        Several kinetic experiments were performed by varying the reaction temperature from  
448        20 to 80 °C, inlet LA concentration from 1.74 to 5.09 mol.L<sup>-1</sup>, inlet butanol concentration  
449        from 5.09 to 9.07 mol.L<sup>-1</sup>, mass of dried enzyme from 50 to 150 mg and residence time  
450        from 1 to 30 minutes.

451        The equilibrium constants were evaluated via the ePC-SAFT equation of state.

452        We evaluated 6 kinetic models based on power law, the classical Ping-Pong Bi-Bi  
453        mechanism and the modified one developed by Mitchell and Krieger. Based on the  
454        Akaike information criterion, we found that the classical Ping-Pong model, including  
455        the inhibition mechanism by butanol and levulinic acid, can fit the experimental  
456        concentrations properly. This model can reasonably predict the experimental  
457        concentration by considering the temperature effect on the rate constant.

458

459 **Declaration of Competing Interest**

460 The authors declare that they have no known competing financial interests or personal  
461 relationships that could have appeared to influence the work reported in this paper.

462 **Acknowledgments**

463 The authors thank INSA Rouen Normandy, University of Rouen Normandy, the Centre  
464 National de la Recherche Scientifique (CNRS), European Regional Development Fund  
465 (ERDF) N° HN0001343, Labex SynOrg (ANR-11-LABX-0029), Carnot Institute I2C, the  
466 graduate school for reasearch XL-Chem (ANR-18-EURE-0020 XL CHEM) and Region  
467 Normandie for their support. This research was funded, in whole or in part, by the ANR  
468 (French National Research Agency) and the DFG (German Research Foundation)  
469 through the project MUST (MicroflUidics for Structure-reactivity relationships aided by  
470 Thermodynamics & kinetics) [ANR-20-CE92-0002 & Project number 446436621].

471

472 **References**

- 473 [1] M.S. Singhvi, D. V. Gokhale, Lignocellulosic biomass: Hurdles and challenges  
474 in its valorization, *Appl. Microbiol. Biotechnol.* 103 (2019) 9305–9320.  
475 <https://doi.org/10.1007/s00253-019-10212-7>.
- 476 [2] Y.N. Guragain, P. V. Vadlani, Renewable Biomass Utilization: A Way Forward  
477 to Establish Sustainable Chemical and Processing Industries, *Clean Technol.* 3  
478 (2021) 243–259. <https://doi.org/10.3390/cleantechnol3010014>.
- 479 [3] P. Zhu, O.Y. Abdelaziz, C.P. Hultberg, A. Riisager, New synthetic approaches  
480 to biofuels from lignocellulosic biomass, *Curr. Opin. Green Sustain. Chem.* 21  
481 (2020) 16–21. <https://doi.org/10.1016/j.cogsc.2019.08.005>.
- 482 [4] X. Lu, L. Lagerquist, K. Eränen, J. Hemming, P. Eklund, L. Estel, S. Leveneur,  
483 H. Grénman, Reductive Catalytic Depolymerization of Semi-industrial Wood-  
484 Based Lignin, *Ind. Eng. Chem. Res.* (2021) [acs.iecr.1c03154](https://doi.org/10.1021/acs.iecr.1c03154).  
485 <https://doi.org/10.1021/acs.iecr.1c03154>.
- 486 [5] W. Schutyser, T. Renders, S. Van Den Bosch, S.F. Koelewijn, G.T. Beckham,  
487 B.F. Sels, Chemicals from lignin: an interplay of lignocellulose fractionation,  
488 depolymerisation, and upgrading, *Chem. Soc. Rev.* 47 (2018) 852–908.  
489 <https://doi.org/10.1039/C7CS00566K>.
- 490 [6] R. Rinaldi, R. Jastrzebski, M.T. Clough, J. Ralph, M. Kennema, P.C.A.  
491 Bruijninx, B.M. Weckhuysen, Paving the Way for Lignin Valorisation: Recent  
492 Advances in Bioengineering, Biorefining and Catalysis, *Angew. Chemie Int. Ed.*  
493 55 (2016) 8164–8215. <https://doi.org/10.1002/ANIE.201510351>.
- 494 [7] K.C. Badgujar, V.C. Badgujar, B.M. Bhanage, A review on catalytic synthesis of

- 495 energy rich fuel additive levulinate compounds from biomass derived levulinic  
496 acid, *Fuel Process. Technol.* 197 (2020) 106213.  
497 <https://doi.org/10.1016/j.fuproc.2019.106213>.
- 498 [8] D. Di Menno Di Bucchianico, Y. Wang, J.-C. Buvat, Y. Pan, V. Casson Moreno,  
499 S. Leveneur, Production of levulinic acid and alkyl levulinates: a process  
500 insight, *Green Chem.* 24 (2022) 614–646. <https://doi.org/10.1039/d1gc02457d>.
- 501 [9] A. Démolis, N. Essayem, F. Rataboul, Synthesis and applications of alkyl  
502 levulinates, *ACS Sustain. Chem. Eng.* 2 (2014) 1338–1352.  
503 <https://doi.org/10.1021/sc500082n>.
- 504 [10] L. Yan, Q. Yao, Y. Fu, Conversion of levulinic acid and alkyl levulinates into  
505 biofuels and high-value chemicals, *Green Chem.* 19 (2017) 5527–5547.  
506 <https://doi.org/10.1039/c7gc02503c>.
- 507 [11] Y. Wang, M. Cipolletta, L. Vernières-Hassimi, V. Casson-Moreno, S. Leveneur,  
508 Application of the concept of Linear Free Energy Relationships to the  
509 hydrogenation of levulinic acid and its corresponding esters, *Chem. Eng. J.* 374  
510 (2019) 822–831. <https://doi.org/10.1016/j.cej.2019.05.218>.
- 511 [12] S. Capecchi, Y. Wang, V. Casson Moreno, C. Held, S. Leveneur, Solvent effect  
512 on the kinetics of the hydrogenation of n-butyl levulinate to  $\gamma$ -valerolactone,  
513 *Chem. Eng. Sci.* 231 (2021) 116315.  
514 <https://doi.org/10.1016/j.ces.2020.116315>.
- 515 [13] D.M. Alonso, S.G. Wettstein, J.A. Dumesic, Gamma-valerolactone, a  
516 sustainable platform molecule derived from lignocellulosic biomass, *Green*  
517 *Chem.* 15 (2013) 584–595. <https://doi.org/10.1039/C3GC37065H>.

- 518 [14] L. Negahdar, M.G. Al-Shaal, F.J. Holzhäuser, R. Palkovits, Kinetic analysis of  
519 the catalytic hydrogenation of alkyl levulinates to  $\gamma$ -valerolactone, *Chem. Eng.*  
520 *Sci.* (2017). <https://doi.org/10.1016/j.ces.2016.11.007>.
- 521 [15] W.R.H. Wright, R. Palkovits, Development of heterogeneous catalysts for the  
522 conversion of levulinic acid to  $\gamma$ -valerolactone, *ChemSusChem*. 5 (2012) 1657–  
523 1667. <https://doi.org/10.1002/cssc.201200111>.
- 524 [16] S. Capecci, Y. Wang, J. Delgado, V. Casson Moreno, M. Mignot, H. Grénman,  
525 D.Y. Murzin, S. Leveneur, Bayesian Statistics to Elucidate the Kinetics of  $\gamma$ -  
526 Valerolactone from n-Butyl Levulinate Hydrogenation over Ru/C, *Ind. Eng.*  
527 *Chem. Res.* 60 (2021) 11725–11736. <https://doi.org/10.1021/acs.iecr.1c02107>.
- 528 [17] J. Delgado, W.N. Vasquez Salcedo, G. Bronzetti, V. Casson Moreno, M.  
529 Mignot, J. Legros, C. Held, H. Grénman, S. Leveneur, Kinetic model  
530 assessment for the synthesis of  $\gamma$ -valerolactone from n-butyl levulinate and  
531 levulinic acid hydrogenation over the synergy effect of dual catalysts Ru/C and  
532 Amberlite IR-120, *Chem. Eng. J.* 430 (2022) 133053.  
533 <https://doi.org/10.1016/j.cej.2021.133053>.
- 534 [18] L. Peng, X. Gao, K. Chen, Catalytic upgrading of renewable furfuryl alcohol to  
535 alkyl levulinates using  $AlCl_3$  as a facile, efficient, and reusable catalyst, *Fuel*.  
536 160 (2015) 123–131. <https://doi.org/10.1016/J.FUEL.2015.07.086>.
- 537 [19] A.F. Peixoto, R. Ramos, M.M. Moreira, O.S.G.P. Soares, L.S. Ribeiro, M.F.R.  
538 Pereira, C. Delerue-Matos, C. Freire, Production of ethyl levulinate fuel  
539 bioadditive from 5-hydroxymethylfurfural over sulfonic acid functionalized  
540 biochar catalysts, *Fuel*. 303 (2021) 121227.  
541 <https://doi.org/10.1016/J.FUEL.2021.121227>.

- 542 [20] E. Christensen, A. Williams, S. Paul, S. Burton, R.L. McCormick, Properties  
543 and Performance of Levulinate Esters as Diesel Blend Components, *Energy*  
544 and *Fuels*. 25 (2011) 5422–5428. <https://doi.org/10.1021/EF201229J>.
- 545 [21] S. Frigo, G. Pasini, G. Caposciutti, M. Antonelli, A.M.R. Galletti, S. Gori, R.  
546 Costi, L. Arnone, Utilisation of advanced biofuel in CI internal combustion  
547 engine, *Fuel*. 297 (2021) 120742. <https://doi.org/10.1016/J.FUEL.2021.120742>.
- 548 [22] D. Di Menno Di Bucchianico, J.C. Buvat, M. Mignot, V. Casson Moreno, S.  
549 Leveneur, Role of solvent the production of butyl levulinate from fructose, *Fuel*.  
550 318 (2022) 123703. <https://doi.org/10.1016/j.fuel.2022.123703>.
- 551 [23] A. Harwardt, K. Kraemer, B. Rüngeler, W. Marquardt, Conceptual Design of a  
552 Butyl-levulinate Reactive Distillation Process by Incremental Refinement,  
553 *Chinese J. Chem. Eng.* 19 (2011) 371–379. [https://doi.org/10.1016/S1004-](https://doi.org/10.1016/S1004-9541(09)60223-8)  
554 [9541\(09\)60223-8](https://doi.org/10.1016/S1004-9541(09)60223-8).
- 555 [24] V. Russo, R. Tesser, C. Rossano, T. Cogliano, R. Vitiello, S. Leveneur, M. Di  
556 Serio, Kinetic study of Amberlite IR120 catalyzed acid esterification of levulinic  
557 acid with ethanol: From batch to continuous operation, *Chem. Eng. J.* 401  
558 (2020) 126126. <https://doi.org/10.1016/J.CEJ.2020.126126>.
- 559 [25] M.A. Tejero, E. Ramírez, C. Fité, J. Tejero, F. Cunill, Esterification of levulinic  
560 acid with butanol over ion exchange resins, *Appl. Catal. A Gen.* 517 (2016) 56–  
561 66. <https://doi.org/10.1016/J.APCATA.2016.02.032>.
- 562 [26] A.F. Peixoto, S.M. Silva, P. Costa, A.C. Santos, B. Valentim, J.M. Lázaro-  
563 Martínez, C. Freire, Acid functionalized coal fly ashes: New solid catalysts for  
564 levulinic acid esterification, *Catal. Today*. 357 (2020) 74–83.  
565 <https://doi.org/10.1016/j.cattod.2019.07.038>.

- 566 [27] S. Dharne, V. V. Bokade, Esterification of levulinic acid to n-butyl levulinate  
567 over heteropolyacid supported on acid-treated clay, *J. Nat. Gas Chem.* 20  
568 (2011) 18–24. [https://doi.org/10.1016/S1003-9953\(10\)60147-8](https://doi.org/10.1016/S1003-9953(10)60147-8).
- 569 [28] K.Y. Nandiwale, V. V. Bokade, Esterification of Renewable Levulinic Acid to n-  
570 Butyl Levulinate over Modified H-ZSM-5, *Chem. Eng. Technol.* 38 (2015) 246–  
571 252. <https://doi.org/10.1002/ceat.201400326>.
- 572 [29] K.Y. Nandiwale, V. V. Bokade, Environmentally benign catalytic process for  
573 esterification of renewable levulinic acid to various alkyl levulinates biodiesel,  
574 *Environ. Prog. Sustain. Energy.* 34 (2015) 795–801.  
575 <https://doi.org/10.1002/ep.12042>.
- 576 [30] K.C. Maheria, J. Kozinski, A. Dalai, Esterification of Levulinic Acid to n-Butyl  
577 Levulinate Over Various Acidic Zeolites, *Catal. Lett.* 2013 14311. 143 (2013)  
578 1220–1225. <https://doi.org/10.1007/S10562-013-1041-3>.
- 579 [31] M. Song, X. Di, Y. Zhang, Y. Sun, Z. Wang, Z. Yuan, Y. Guo, The effect of  
580 enzyme loading, alcohol/acid ratio and temperature on the enzymatic  
581 esterification of levulinic acid with methanol for methyl levulinate production: A  
582 kinetic study, *RSC Adv.* 11 (2021) 15054–15059.  
583 <https://doi.org/10.1039/d1ra01780b>.
- 584 [32] G.D. Yadav, I. V. Borkar, Kinetic Modeling of Immobilized Lipase Catalysis in  
585 Synthesis of n-Butyl Levulinate†, *Ind. Eng. Chem. Res.* 47 (2008) 3358–3363.  
586 <https://doi.org/10.1021/IE800193F>.
- 587 [33] V.N. Emel'yanenko, E. Altuntepe, C. Held, A.A. Pimerzin, S.P. Verevkin,  
588 Renewable platform chemicals: Thermochemical study of levulinic acid esters,  
589 *Thermochim. Acta.* 659 (2018) 213–221.



- 590 <https://doi.org/10.1016/j.tca.2017.12.006>.
- 591 [34] K. V. Bhavsar, G.D. Yadav, n-Butyl levulinate synthesis using lipase catalysis:  
592 comparison of batch reactor versus continuous flow packed bed tubular  
593 microreactor, *J. Flow Chem.* 8 (2018) 97–105. [https://doi.org/10.1007/s41981-](https://doi.org/10.1007/s41981-018-0014-5)  
594 [018-0014-5](https://doi.org/10.1007/s41981-018-0014-5).
- 595 [35] L. Zhou, Y. He, L. Ma, Y. Jiang, Z. Huang, L. Yin, J. Gao, Conversion of  
596 levulinic acid into alkyl levulinates: Using lipase immobilized on meso-molding  
597 three-dimensional macroporous organosilica as catalyst, *Bioresour. Technol.*  
598 247 (2018) 568–575. <https://doi.org/10.1016/J.BIORTECH.2017.08.134>.
- 599 [36] S. Zhai, L. Zhang, X. Zhao, Q. Wang, Y. Yan, C. Li, X. Zhang, Enzymatic  
600 synthesis of a novel solid–liquid phase change energy storage material based  
601 on levulinic acid and 1,4-butanediol, *Bioresour. Bioprocess.* 9 (2022) 1–10.  
602 <https://doi.org/10.1186/s40643-022-00502-w>.
- 603 [37] K.C. Badgujar, V.C. Badgujar, B.M. Bhanage, Lipase as a green and  
604 sustainable material for production of levulinate compounds: State of the art,  
605 *Mater. Sci. Energy Technol.* (2022). <https://doi.org/10.1016/j.mset.2022.02.005>.
- 606 [38] R. Gérardy, D.P. Debecker, J. Estager, P. Luis, J.C.M. Monbaliu, Continuous  
607 Flow Upgrading of Selected C2–C6 Platform Chemicals Derived from Biomass,  
608 *Chem. Rev.* 120 (2020) 7219–7347.  
609 <https://doi.org/10.1021/ACS.CHEMREV.9B00846>.
- 610 [39] H. Zhang, Y. Bai, N. Zhu, J. Xu, Microfluidic reactor with immobilized enzyme-  
611 from construction to applications: A review, *Chinese J. Chem. Eng.* 30 (2021)  
612 136–145. <https://doi.org/10.1016/J.CJCHE.2020.12.011>.

- 613 [40] C.J. Taylor, J.A. Manson, G. Clemens, B.A. Taylor, T.W. Chamberlain, R.A.  
614 Bourne, Modern advancements in continuous-flow aided kinetic analysis,  
615 *React. Chem. Eng.* (2022). <https://doi.org/10.1039/d1re00467k>.
- 616 [41] H. Hajifatheali, E. Ahmadi, A. Wojtczak, Z. Jaglicic, The synthesis of N-  
617 methylbis[2-(dodecylthio)ethyl]amine (SNS) and investigation of its efficiency  
618 as new mononuclear catalyst complex in copper-based ATRP, *Macromol. Res.*  
619 2015 2311. 23 (2015) 977–985. <https://doi.org/10.1007/S13233-015-3132-Z>.
- 620 [42] L.K. Doraiswamy, D.G. Tajbl, *Laboratory Catalytic Reactors*, *Catal. Rev.* 10  
621 (1974) 177–219. <https://doi.org/10.1080/01614947408079629>.
- 622 [43] J.-M. Commenge, M. Saber, L. Falk, Methodology for multi-scale design of  
623 isothermal laminar flow networks, *Chem. Eng. J.* 173 (2011) 541–551.  
624 <https://doi.org/10.1016/J.CEJ.2011.07.060>.
- 625 [44] A.A. Hassankiadeh, *Dynamic Assessment and Optimization of Catalytic*  
626 *Hydroprocessing Process: Sensitivity Analysis and Practical Tips*, University of  
627 Newfoundland, 2021.
- 628 [45] S. Leveneur, J. Wärnå, K. Eränen, T. Salmi, Green process technology for  
629 peroxycarboxylic acids: Estimation of kinetic and dispersion parameters aided  
630 by RTD measurements: Green synthesis of peroxycarboxylic acids, *Chem.*  
631 *Eng. Sci.* 66 (2011) 1038–1050. <https://doi.org/10.1016/j.ces.2010.12.005>.
- 632 [46] J. Villermaux, *Génie de la réaction chimique*, Technip, Tec & Doc Lavoisier,  
633 Paris, 1993.  
634 <http://www.lavoisier.fr/livre/notice.asp?depuis=e.lavoisier.fr&id=978285206759>  
635 2.

- 636 [47] M. Ravelo, M. Wojtusik, M. Ladero, F. García-Ochoa, Synthesis of ibuprofen  
637 monoglyceride in solventless medium with novozym®435: Kinetic analysis,  
638 Catalysts. 10 (2020) 76. <https://doi.org/10.3390/catal10010076>.
- 639 [48] C.R. Wilke, P. Chang, Correlation of diffusion coefficients in dilute solutions,  
640 AIChE J. 1 (1955) 264–270. <https://doi.org/10.1002/aic.690010222>.
- 641 [49] H. Ariba, Y. Wang, C. Devouge-Boyer, R.P. Stateva, S. Leveneur,  
642 Physicochemical Properties for the Reaction Systems: Levulinic Acid, Its  
643 Esters, and  $\gamma$ -Valerolactone, J. Chem. Eng. Data. 65 (2020) 3008–3020.  
644 <https://doi.org/10.1021/acs.jced.9b00965>.
- 645 [50] D.M. Chesterfield, P.L. Rogers, E.O. Al-Zaini, A.A. Adesina, Production of  
646 biodiesel via ethanolysis of waste cooking oil using immobilised lipase, Chem.  
647 Eng. J. 207–208 (2012) 701–710. <https://doi.org/10.1016/J.CEJ.2012.07.039>.
- 648 [51] C. Ortiz, M.L. Ferreira, O. Barbosa, J.C.S. Dos Santos, R.C. Rodrigues, Á.  
649 Berenguer-Murcia, L.E. Briand, R. Fernandez-Lafuente, Novozym 435: The  
650 “perfect” lipase immobilized biocatalyst?, Catal. Sci. Technol. 9 (2019) 2380–  
651 2420. <https://doi.org/10.1039/c9cy00415g>.
- 652 [52] D. Kowalczykiewicz, K. Szymańska, D. Gillner, A.B. Jarzębski, Rotating bed  
653 reactor packed with heterofunctional structured silica-supported lipase.  
654 Developing an effective system for the organic solvent and aqueous phase  
655 reactions, Microporous Mesoporous Mater. 312 (2021) 110789.  
656 <https://doi.org/10.1016/j.micromeso.2020.110789>.
- 657 [53] H. Zhao, Z. Song, Migration of reactive trace compounds from Novozym® 435  
658 into organic solvents and ionic liquids, Biochem. Eng. J. 49 (2010) 113–118.  
659 <https://doi.org/10.1016/j.bej.2009.12.004>.

- 660 [54] J. Gross, G. Sadowski, Perturbed-Chain SAFT: An Equation of State Based on  
661 a Perturbation Theory for Chain Molecules, *Ind. Eng. Chem. Res.* 40 (2001)  
662 1244–1260. <https://doi.org/10.1021/IE0003887>.
- 663 [55] M. Lemberg, G. Sadowski, Predicting the Solvent Effect on Esterification  
664 Kinetics, *ChemPhysChem.* 18 (2017) 1977–1980.  
665 <https://doi.org/10.1002/cphc.201700507>.
- 666 [56] E. Altuntepe, V.N. Emel'yanenko, M. Forster-Rotgers, G. Sadowski, S.P.  
667 Verevkin, C. Held, Thermodynamics of enzyme-catalyzed esterifications: II.  
668 Levulinic acid esterification with short-chain alcohols, *Appl. Microbiol.*  
669 *Biotechnol.* 101 (2017) 7509–7521. [https://doi.org/10.1007/s00253-017-8481-](https://doi.org/10.1007/s00253-017-8481-4)  
670 4.
- 671 [57] C. Held, G. Sadowski, Thermodynamics of Bioreactions, *Annu. Rev. Chem.*  
672 *Biomol. Eng.* 7 (2016) 395–414. [https://doi.org/10.1146/annurev-chembioeng-](https://doi.org/10.1146/annurev-chembioeng-080615-034704)  
673 080615-034704.
- 674 [58] F. Tumakaka, G. Sadowski, Application of the Perturbed-Chain SAFT equation  
675 of state to polar systems, in: *Fluid Phase Equilib.*, American Chemical Society,  
676 2004: pp. 233–239. <https://doi.org/10.1016/j.fluid.2002.12.002>.
- 677 [59] D. Fuchs, J. Fischer, F. Tumakaka, G. Sadowski, Solubility of Amino Acids:  
678 Influence of the pH value and the Addition of Alcoholic Cosolvents on Aqueous  
679 Solubility, *Ind. Eng. Chem. Res.* 45 (2006) 6578–6584.  
680 <https://doi.org/10.1021/IE0602097>.
- 681 [60] G.D. Yadav, S. V. Pawar, Synergism between microwave irradiation and  
682 enzyme catalysis in transesterification of ethyl-3-phenylpropanoate with n-  
683 butanol, *Bioresour. Technol.* 109 (2012) 1–6.

- 684 <https://doi.org/10.1016/j.biortech.2012.01.030>.
- 685 [61] S.R. Bansode, M.A. Hardikar, V.K. Rathod, Evaluation of reaction parameters  
686 and kinetic modelling for Novozym 435 catalysed synthesis of isoamyl butyrate,  
687 J. Chem. Technol. Biotechnol. 92 (2017) 1306–1314.  
688 <https://doi.org/10.1002/jctb.5125>.
- 689 [62] S.A. Zulkeflee, S.A. Sata, F.S. Rohman, N. Aziz, Modelling of immobilized  
690 *Candida rugosa* lipase catalysed esterification process in batch reactor  
691 equipped with temperature and water activity control system, Biochem. Eng. J.  
692 161 (2020) 107669. <https://doi.org/10.1016/j.bej.2020.107669>.
- 693 [63] D.A. Mitchell, N. Krieger, Looking through a new lens: Expressing the Ping  
694 Pong bi bi equation in terms of specificity constants, Biochem. Eng. J. 178  
695 (2022) 108276. <https://doi.org/10.1016/j.bej.2021.108276>.
- 696 [64] C.G. Lopresto, V. Calabrò, J.M. Woodley, P. Tufvesson, Kinetic study on the  
697 enzymatic esterification of octanoic acid and hexanol by immobilized *Candida*  
698 *antarctica* lipase B, J. Mol. Catal. B Enzym. 110 (2014) 64–71.  
699 <https://doi.org/10.1016/j.molcatb.2014.09.011>.
- 700 [65] M.N. Varma, G. Madras, Kinetics of synthesis of butyl butyrate by esterification  
701 and transesterification in supercritical carbon dioxide, J. Chem. Technol.  
702 Biotechnol. 83 (2008) 1135–1144. <https://doi.org/10.1002/jctb.1897>.
- 703 [66] M. Rizzi, P. Stylos, A. Riek, M. Reuss, A kinetic study of immobilized lipase  
704 catalysing the synthesis of isoamyl acetate by transesterification in n-hexane,  
705 Enzyme Microb. Technol. 14 (1992) 709–714. [https://doi.org/10.1016/0141-](https://doi.org/10.1016/0141-0229(92)90110-A)  
706 [0229\(92\)90110-A](https://doi.org/10.1016/0141-0229(92)90110-A).

- 707 [67] M. Caracotsios, W.E. Stewart, Sensitivity analysis of initial value problems with  
708 mixed odes and algebraic equations, *Comput. Chem. Eng.* 9 (1985) 359–365.  
709 [https://doi.org/10.1016/0098-1354\(85\)85014-6](https://doi.org/10.1016/0098-1354(85)85014-6).
- 710 [68] W.E. Stewart, M. Caracotsios, *Computer-Aided Modeling of Reactive Systems*,  
711 First, New Jersey, 2008. <https://doi.org/10.1002/9780470282038>.
- 712 [69] G. Buzzi-Ferraris, Planning of experiments and kinetic analysis, *Catal. Today*.  
713 52 (1999) 125–132. [https://doi.org/10.1016/S0920-5861\(99\)00070-X](https://doi.org/10.1016/S0920-5861(99)00070-X).
- 714 [70] M.A. McDonald, L. Bromig, M.A. Grover, R.W. Rousseau, A.S. Bommarius,  
715 Kinetic model discrimination of penicillin G acylase thermal deactivation by  
716 non-isothermal continuous activity assay, *Chem. Eng. Sci.* 187 (2018) 79–86.  
717 <https://doi.org/10.1016/j.ces.2018.04.046>.
- 718 [71] K. Toch, J.W. Thybaut, G.B. Marin, A systematic methodology for kinetic  
719 modeling of chemical reactions applied to n-hexane hydroisomerization, *AIChE*  
720 *J.* 61 (2015) 880–892. <https://doi.org/10.1002/aic.14680>.
- 721
- 722